

Coulomb blockade model of permeation and selectivity in biological ion channels

I.Kh. Kaufman¹, P.V.E. McClintock¹, R.S. Eisenberg³

¹Department of Physics, Lancaster University, Lancaster LA1 4YB, UK.

E-mail: i.kaufman@lancaster.ac.uk

E-mail: p.v.e.mcclintock@lancaster.ac.uk

³Department of Molecular Biophysics and Physiology, Rush Medical College, 1750 West Harrison, Chicago, IL 60612, USA.

E-mail: beisenbe@rush.edu

Abstract.

Biological ion channels are protein nanotubes embedded in, and passing through, the bilipid membranes of cells. Physiologically, they are of crucial importance in that they allow ions to pass into and out of cells, fast and efficiently, though in a highly selective way. Here we show that the conduction and selectivity of calcium/sodium ion channels can be described in terms of ionic Coulomb blockade in a simplified electrostatic and Brownian dynamics model of the channel. The Coulomb blockade phenomenon arises from the discreteness of electrical charge, the strong electrostatic interaction, and an electrostatic exclusion principle. The model predicts a periodic pattern of Ca^{2+} conduction *vs.* the fixed charge Q_f at the selectivity filter (conduction bands) with a period equal to the ionic charge. It thus provides **provisional** explanations of **some** observed and modelled conduction and valence selectivity phenomena, including the anomalous mole fraction effect and the calcium conduction bands. Ionic Coulomb blockade and resonant conduction are similar to electronic Coulomb blockade and resonant tunnelling in quantum dots. The same considerations may also be applicable to other kinds of channel, as well as to charged artificial nanopores.

PACS numbers: 87.16.Vy, 41.20.Cv, 05.40.-a, 05.30.-d, 87.10.Mn

1. Introduction

Biological ion channels are natural nanopores providing fast and highly selective permeation of physiologically important ions (e.g. cations such as Na^+ , K^+ and Ca^{2+}) through the bilipid membranes of biological cells [1–3]. The channel proteins carrying the pores are embedded in the cellular membrane, and are complicated structures consisting of thousands of atoms.

More than three decades after their discovery, and following a vast number of experiments, a great deal is now known about ion channels. Yet there remain many features of their function – including some quite basic features – that are still not properly understood. Examples include: the *selectivity* in which e.g. a calcium channel favours Ca^{2+} over Na^+ by up to 1000:1, even though the ions are essentially the same size; that this selectivity is combined with *fast permeation* in which the ion goes through the channel almost at the rate of free diffusion (as though the channel were an open hole); the *anomalous mole fraction effect* (AMFE) where, in a pure NaCl solution, a Na^+ ion can pass easily through a calcium channel, but its passage is blocked by tiny traces of Ca^{2+} ; the exact role of the *fixed electric charge* at the so-called selectivity filter in determining the selectivity; and, associated with that, the mechanism by which *mutations* that alter the fixed charge can result either in destruction of the channel, so that it no longer conducts, or in conversion of e.g. a sodium channel into a calcium channel or *vice versa*. We will account for these and other experimentally observed features of channel conduction in terms of a novel vision of the permeation process inspired by well-understood phenomena in a quite different area of physics, associated with quantum dots and tunnel diodes.

The conduction and selectivity of a cation-selective channel are determined by the ions' movements and interactions inside a short, narrow selectivity filter lined with negatively-charged protein residues that provide the net fixed negative charge Q_f ; correspondingly, anion-conducting channels possess positive fixed charge [1,4]. Ions in solution are surrounded by hydration shells with associated dehydration potential barriers that are also crucial for selectivity in many cases [5–9]. Selectivity frequently involves a “knock on” mechanism or, more generally, the correlated motion of several ions [10–13]. The protein residues forming the “locus” of the selectivity filter are amino acids, of which aspartate (D) and glutamate (E) have negatively charged side chains ($Q_f = -1e$ where e is the proton charge), lysine (K) has a positively charged side chain ($Q_f = +1e$), and alanine (A) has a neutral side chain. The nominal Q_f value is defined by which amino acid residues are present. Calcium L-type channels possess EEEE selectivity filter loci ($Q_f \simeq -4e$) [14–16]. Mammalian Na^+ channels have DEKA inner site loci (and DDEE outer sites) [1, 17] and hence different Q_f . Bacterial NaChBac [18] and NavAb [19, 20] Na^+ channels have selectivity filters with EEEE loci like Ca^{2+} channels *but* select Na^+ ions over Ca^{2+} : an apparent anomaly that awaits explanation.

The modern study of ion channels is based on the existence of the distinct open and closed states of channels, evident in thousands of experiments as discrete levels of current

flow measured from individual channel proteins [21]. Site-directed mutagenesis provides a method for systematically varying the structure and net charge of their selectivity filter loci. The resultant changes in conduction and selectivity as functions of Q_f can then be measured by use of the patch-clamp technique. Such mutant studies [18, 22–29] have demonstrated that Q_f is a key determinant of conduction and selectivity in the calcium/sodium family of channels, with the $\text{Ca}^{2+}/\text{Na}^+$ selectivity growing with increasing $|Q_f|$ [30–33]. However, the underlying mechanism has remained obscure.

Discovery of the structures of the bacterial potassium KcsA [34] and sodium NavAb [19] channels and the application of all-atom molecular dynamics simulations [20, 28, 35–37] have yielded deep insight into fine details of the ionic permeation processes, including the reproduction of currents [38, 39]. However, a *multi-scale* analysis is still needed [40–42] to build up a full picture. Self-consistent electrostatic and Brownian dynamics simulations [15, 30, 43–45] describe ionic motion as an electro-diffusion process, leading to fast and direct estimation of the currents under non-equilibrium conditions. Such simulations have shown very clearly that the permeation and selectivity features of many channels are defined by just the basic electrostatics of narrow water-filled channels, rather than by the details of the channel structures themselves.

The discreteness of the ionic charge plays a significant role in ion channel conduction [8, 46–48]. An electrostatic theory of ionic transport in water-filled periodically-charged nanopores [49, 50], treating the ions as a 1D Coulomb gas [50], revealed ion-exchange through low-barrier phase transitions as the ion concentration and Q_f were varied [51]. It has recently been shown that nanopores can exhibit ionic Coulomb blockade [52], an electrostatic phenomenon similar to electronic Coulomb blockade in mesoscopic systems [53–56].

Our earlier simulations of a simple electrostatic model of calcium/sodium ion channels revealed a periodic set of Ca^{2+} conduction-bands and stop-bands as a function of the fixed charge Q_f at the selectivity filter [57–59] similar to transitions [51]. The energetics of that phenomenon has been derived from electrostatics as single- and multi-ion barrier-less conduction and results were compared with the experimental data available to date [58, 59].

In this paper we demonstrate that the origin of these conduction bands lies in ionic Coulomb blockade [52], closely similar to its electronic counterpart in quantum dots [53]. We thus introduce a Coulomb blockade model of permeation and selectivity in biological ion channels, describing them as discrete electrostatic devices [56]. The applicability of Coulomb blockade to biological ion channels follows naturally from an earlier discussion of the crucial role of electrostatics and the suggestion that there might be “eigenstates” for conduction [60, 61] in biological ion channels. We will show that the Coulomb blockade model predicts the positions and shapes of the conduction bands, defines the channel occupancy as a Fermi-Dirac distribution, and thereby provides an explanation of divalent block and AMFE, including the exponential dependence of the divalent block threshold IC_{50} on Q_f .

We will focus on the sodium/calcium family of channels including the voltage-

gated Ca^{2+} [14, 28] and Na^+ channels [19, 62]. These channels exhibit strong valence selectivity and can undergo a wide range of transformations as the result of site-directed mutagenesis, enabling us to test many of the predictions of our model. The picture that we will develop may, however, be more generally applicable. Section 2 describes a generic model of calcium/sodium channels, its geometry (2.1), electrostatics (2.2), Brownian dynamics (2.3) and validity (2.4). Section 3 introduces and verifies the ionic Coulomb blockade model of ion channel conduction and selectivity; it reviews multi-ion conduction bands (3.1), describes Coulomb blockade model (3.2), identifies real channels and mutants (3.3), derives the shape of Coulomb blockade oscillations (3.4) and explains the selectivity and AMFE (3.5). Subsection 3.6 contains further considerations. Section 4 draws the results together and presents concluding remarks.

In what follows, with SI units e is the proton charge, T the temperature, z the ionic valence, k_B Boltzmann's constant and ε_0 the electric permittivity of the vacuum. We use dimensionless units for energy assuming $k_B T = 1$.

2. A generic electrostatic and Brownian dynamics model of the Calcium channel

2.1. Geometry and general features of the model

Figure 1(a) shows the generic, self-consistent, electrostatic model of the selectivity filter of a calcium/sodium channel whose properties we will analyse. We consider it as a negatively-charged, axisymmetric, water-filled, cylindrical pore through the protein hub in the cellular membrane; and, to match the dimensions of the selectivity filters of the $\text{Na}^+/\text{Ca}^{2+}$ channels on which we focus, we suppose it to be of radius $R = 0.3$ nm and length $L = 1.6$ nm [14, 15, 63]. The x -axis is coincident with the channel axis, with $x = 0$ in the center of channel. There is a centrally-placed, uniformly-charged, rigid ring of negative charge $0 \leq |Q_f/e| \leq 7$ embedded in the wall at $R_Q = R$. The left-hand bath, modeling the extracellular space, contains non-zero concentrations of Ca^{2+} and/or Na^+ ions. For the Brownian dynamics simulations, the computational domain length $L_d = 10$ nm, its radius $R_d = 10$ nm, the grid size $h = 0.05$ nm, and a potential difference in the range $0 - 25$ mV (corresponding to the depolarized membrane state) was applied between the left and right domain boundaries.

The mobile sodium and calcium ions are described as charged spheres of radius $R_i \approx 0.1$ nm for both ions (allowing use of the implicit solvent model [64, 65] with negligible ion radii), with diffusion coefficients of $D_{\text{Na}} = 1.33 \times 10^{-9}$ m²/s [15, 66] and $D_{\text{Ca}} = 0.79 \times 10^{-9}$ m²/s [15], respectively.

We take both the water and the protein to be homogeneous continua describable by relative permittivities $\varepsilon_w = 80$ and $\varepsilon_p = 2$, respectively, together with an implicit model of ion hydration whose validity is discussed elsewhere [58]. We approximate ε_w , D_{Na} , and D_{Ca} as being equal to their bulk values throughout the whole computational domain (see below, section 2.4).

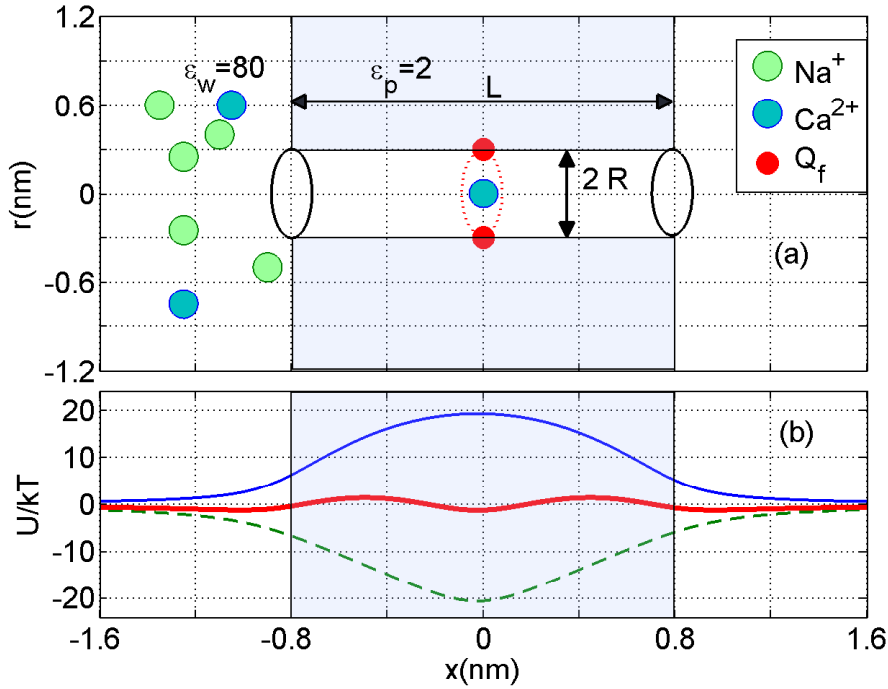


Figure 1. (a) Generic electrostatic model of the selectivity filter of a Ca^{2+} or Na^+ channel. It is treated as an axisymmetric, water-filled, cylindrical pore of radius $R = 0.3\text{nm}$ and length $L = 1.6\text{nm}$ through the protein hub in the cellular membrane. A centrally-placed, uniform, rigid ring of negative charge Q_f in the range $0 \leq |Q_f/e| \leq 7$ is embedded in the wall at $R_Q = R$. Ions inside the channel move in single file along its axis. (b) Energetics of a moving Ca^{2+} ion for fixed charge $Q_f = -1e$. The dielectric self-energy barrier U_s (blue solid line) is balanced by site attraction (green dashed line) resulting in an almost barrier-less energy profile (red solid line).

2.2. Self-consistent electrostatics of the model

The electrostatic potential U for an ion, and the potential gradients, were derived by numerical solution of Poisson's electrostatic equation within the computational domain shown in figure 1:

$$-\nabla \cdot (\epsilon_0 \epsilon \nabla \phi) = \rho_0 + \sum_i e z_i n_i \quad (\text{Poisson's equation}) \quad (1)$$

where ϵ is the relative permittivity of the medium (water or protein), ρ_0 is the density of fixed charge, z_i is the charge number (valence), and n_i is the number density of moving ions.

Self-consistent electrostatics within the narrow, water-filled, channel in the protein differs significantly from bulk electrostatics [49, 67, 68]. The huge gradient between $\epsilon_w = 80$ and $\epsilon_p = 2$, the discreteness of ionic charge and the specific channel geometry, lead to permeation, quasi-1D axial behaviour of ions inside the channel [49, 50, 69], and hence to single-filing. Consequently, we use a 1D dynamical model to simulate the axial single-file movement of cations (only) inside the selectivity filter and in its close vicinity.

Coulomb blockade model of permeation and selectivity in biological ion channels 6

Figure 1(b) shows axial single-ion potential energy profiles for $Q_f = -1e$, including the repulsive self-energy barrier U_s and the attraction energy U_a attributable to the fixed negative charge. The dielectric self-energy U_s plays a crucial role in controlling ion permeation through the narrow channel. It will be shown below that U_s defines the strength of Coulomb blockade for an ion of particular valence z , and that it determines the condition for strong valence selectivity [30, 58]. The site attraction is proportional to $z \times Q_f$, so that a variation of Q_f can significantly change the resultant profile. In particular for $Q_f \simeq -1e$, the self-potential barrier of the dielectric boundary force can be balanced by electrostatic attraction to the fixed charge Q_f , resulting in almost barrier-less conduction [58].

2.3. Brownian dynamics simulation of the ionic current

The ions' motion through a channels can be described as an electro-diffusion process and investigated through Brownian dynamics simulations [15, 30, 44, 45, 57, 70–73] of the ionic trajectories. Taking account of the single-filing required by electrostatics, we can solve the over-damped, time-discretized, Langevin equation numerically. An axial step Δx_i of the i -th ion is defined as [74],

$$\Delta x_i = -zeD_i \nabla_x \phi(x_i) \Delta t + \sqrt{2D_i \Delta t} \xi_i(t) \quad (\text{Langevin equation}) \quad (2)$$

where D_i is the ionic diffusion coefficient, Δt is the time step, $\xi_i(t)$ is normalized white noise, z_i is the valence of the i -th ion, and the potential $\phi(x_i)$ is calculated self-consistently from (1) at each simulation step.

Brownian dynamics simulations of the ion current J and occupancy P were performed separately for CaCl_2 and NaCl solutions, and also for a mixed-salt configuration, with concentrations $[\text{Na}] = 30\text{mM}$ and $20\mu\text{M} \leq [\text{Ca}] \leq 80\text{mM}$.

2.4. Validity and limitations of the generic model

Our reduced model obviously represents a considerable simplification of the actual electrostatics and dynamics of moving ions and water molecules within the narrow selectivity filter. The validity and range of applicability of this kind of model have been discussed in detail elsewhere [35, 58, 75, 76]. The most significant simplifications are probably: the use of continuum electrostatics; the use of the implicit solvent model; the use of Brownian dynamics with uncorrelated noise sources for the charged particles; and the assumption of 1D (i.e. single-file) movement of ions inside the selectivity filter. We can partially accommodate these simplifications by use of *effective values* [58].

3. Coulomb blockade model of permeation and selectivity

In this section we introduce the Coulomb blockade picture of permeation and selectivity and show that the phenomenon manifests itself in the model of figure 1 when its geometrical parameters are appropriate for calcium/sodium channels. We

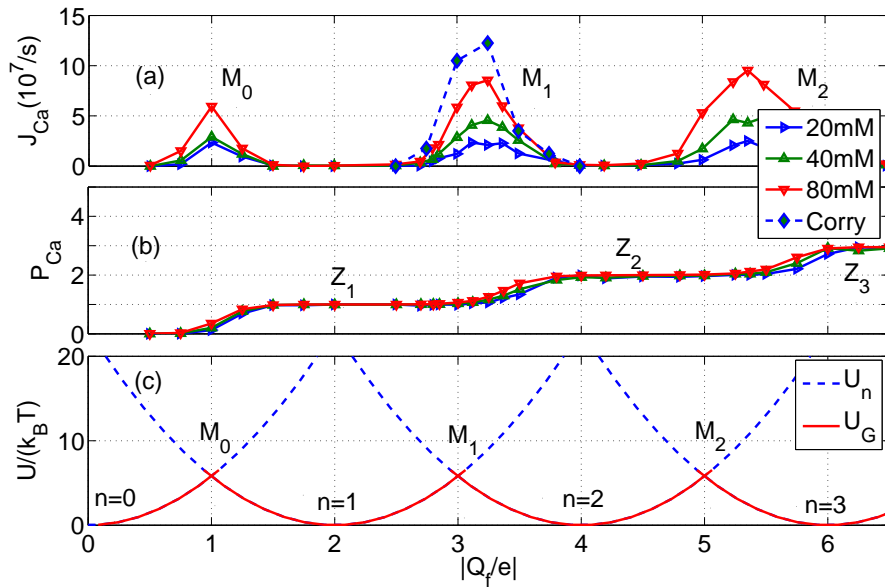


Figure 2. Multi-ion Ca^{2+} conduction and occupancy in the $\text{Ca}^{2+}/\text{Na}^+$ channel model *vs.* the effective fixed charge Q_f ; the Brownian dynamics (BD) simulation results (a),(b) are reworked from [57, 59]. (a) Plots of the Ca^{2+} current J_{Ca} for pure Ca^{2+} baths of concentration 20, 40 and 80mM. The BD results of Corry *et al* [15] are shown for comparison (blue, dashed, diamonds, in arbitrary units). (b) The channel occupancy P_{Ca} . (c) Plots of the electrostatic energy U_n (blue, dashed) and the ground state (i.e. minimum) energy $U_G = \min_n(U_n)$ (red, solid) *vs.* Q_f for channels with $n = 0, 1, 2, 3$. Ca^{2+} ions inside. The conduction bands M_0, M_1, M_2 and the stop bands Z_1, Z_2, Z_3 (indicated by labels) are discussed in the text.

will show that the model describes well both the simulated conduction bands and many experimentally-measured phenomena of valence selectivity in calcium/sodium channels. The Coulomb blockade model provides significant generalisation of our earlier explanation of conduction bands [58] and connects them with mesoscopic transport and single-electron devices [52, 54, 56].

We start by reviewing the main outcome of our earlier Brownian dynamics simulations of conduction bands [57, 58] in order to summarise some of the results that need to be explained including, in particular, the observation of conduction bands.

3.1. Multi-ion conduction bands

Figures 2(a),(b) and 3(a),(b) present the Brownian dynamics results [57–59] for permeation of the model channel figure 1(a) by calcium and sodium ions, respectively, in pure baths of different concentration, plotted in each case as a function of Q_f .

Figure 2(a) exhibits a sequence of narrow conduction bands M_0, M_1, M_2 , separated by stop-bands of almost zero-conductance centred on the blockade points Z_1, Z_2, Z_3 . Figure 2(b) shows that the M_n peaks in J_{Ca} correspond to transition regimes where the channel occupancy P_{Ca} jumps from one integer value to the next, and that the

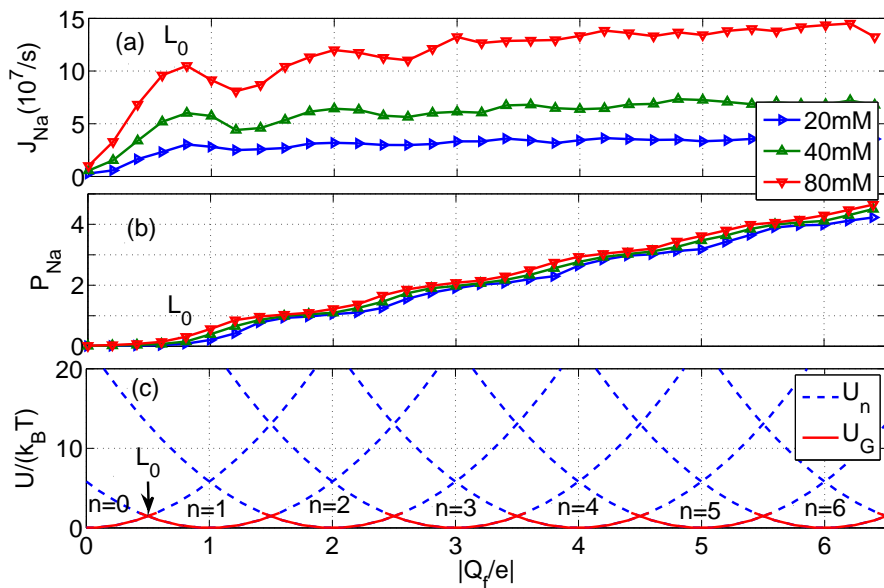


Figure 3. Multi-ion Na⁺ conduction and occupancy in the Ca²⁺/Na⁺ channel model *vs.* the effective fixed charge Q_f ; the Brownian dynamics simulation results (a),(b) are reworked from [59]. (a) Plots of the Na⁺ current J_{Na} for pure Na⁺ baths of concentration 20, 40 and 80mM. (b) The occupancy P_{Na} . (c) Plots of the electrostatic energy U_n (blue, dashed) and resulting oscillations of the ground state energy $U_G = \min_n(U_n)$ (red, solid) *vs.* Q_f for channels with $n = 0, 1, 2, \dots, 6$ Na⁺ ions inside. The conduction band L_0 is discussed in the text.

stop-bands correspond to saturated regions with integer $P_{Ca} = 1, 2, 3, \dots$

The band M_0 corresponds to single-ion low-barrier conduction (see red curve in figure 1(b)). Band M_1 corresponds to double-ion knock-on conduction, which is well-established for L-type Ca²⁺ channels [14, 77, 78]; a similar peak was obtained by Corry *et al* [15] in Brownian dynamics simulations of the Ca²⁺ channel. Band M_2 corresponds to triple-ion conduction, a process that can be identified with the permeation of ryanodine receptor calcium channels [7] (see Table 1 below for further detail). These bands can be considered as examples of self-organization in ion channels [16, 73].

Comparison of the J_{Ca} and P_{Ca} plots in figures 2(a) and (b) shows that for the M_n points near which conduction occurs, $Q_f = -ze(n + 1/2)$; whereas the non-conducting regions of constant P correspond to Z_n points with $Q_f = -zen$, i.e. to the neutralized state [59]. These bands will be interpreted below as *strong Coulomb blockade*.

Figures 3 (a) and (b) plot the equivalent results for sodium ions in pure NaCl baths of different concentration showing (a) the sodium current and (b) the occupancy as functions of Q_f . The current J_{Na} exhibits a single-ion peak L_0 that would appear to be analogous to the calcium conduction band M_0 of figure 2(a). For larger Q_f there are weak, strongly overlapping, conduction bands between which the current does not fall to zero, making the sodium conductance relatively independent of Q_f . The separations of the J_{Na} band maxima are approximately half the size of those for the calcium bands,

1
2
3 *Coulomb blockade model of permeation and selectivity in biological ion channels* 9

4 reflecting the charge difference between Na^+ and Ca^{2+} ions. We will refer to this scenario
5 as an example of *weak Coulomb blockade*.
6

7 Figures 2(c) and 3(c) plot the ground state energies characteristic of Coulomb
8 blockade graphs [56]. They will be discussed in the next section. Note that we use
9 *ground state* in the physics sense, implying the state of minimum energy.
10
11

12 3.2. Coulomb blockade oscillations of conductance

13 We are now in position to introduce the Coulomb blockade model of conduction and
14 selectivity in $\text{Ca}^{2+}/\text{Na}^+$ ion channels. We will find that it is able to account for the
15 pattern of calcium and sodium bands seen in figures 2 and 3 in terms of strong and
16 weak *Coulomb blockade oscillations* [55], respectively .
17

18 The discreteness and entity of the ionic charge allow to us to introduce exclusive
19 “eigenstates” $\{n\}$ of the channel for fixed integer numbers of ions inside its selectivity
20 filter, with total electrostatic energy U_n . The transition $\{n\} \rightarrow \{n+1\}$ corresponds to
21 the entry of a new ion, whereas $\{n\} \rightarrow \{n-1\}$ corresponds to the escape of a trapped
22 ion. The n ions’ eigenstates form a discrete exclusive set of $\{n\}$ -states [79] :
23

$$24 \quad n = \{0, 1, 2, \dots\} \quad \sum_n \theta_n = 1; \quad P_c = \sum_n n\theta_n, \quad (3)$$

25 The *electrostatic exclusion principle* (3) leads to Fermi-Dirac statistical distributions
26 [80] for θ_n and P_c , as will be derived below.
27

28 The total energy U_n for a channel in state $\{n\}$ can be expressed as:
29

$$30 \quad U_n = U_{n,s} + U_{n,a} + U_{n,int} \quad (4)$$

31 where $U_{n,s}$ is the self-energy, $U_{n,a}$ is the energy of attraction, and $U_{n,int}$ is the ions’
32 mutual interaction energy.
33

34 We approximate U_n as the dielectric self-energy $U_{n,s}$ of the excess charge Q_n , based
35 on the assumption that both the ions and Q_f are located within the central part of the
36 selectivity filter, so that application of Gauss’s theorem to the n similar ions captured
37 within its volume gives a Coulomb blockade-like quadratic dependence of U_n on Q_f [51]:
38

$$39 \quad U_n = \frac{Q_n^2 L}{8\pi\epsilon_0\epsilon_w R^2} = \frac{Q_n^2}{2C_s} \quad (\text{Electrostatic energy})$$

$$40 \quad Q_n = zen + Q_f \quad (\text{Excess charge}). \quad (5)$$

41 Here, C_s stands for the geometry-dependent self-capacitance of the channel, and Q_n
42 represents the excess charge at the selectivity filter for the n ions as a function of Q_f .
43 A binomial expansion Q_n^2 in (5) gives first approximations for $U_{n,s}$, $U_{n,a}$ and $U_{n,int}$ that
44 are consistent with the energetics analysis in [58] and with the 1D Coulomb gas model
45 of ion-ion and ion-fixed charge interactions [49, 50]. A more realistic account of the
46 interactions would result in corrections to (5) and to the formulæ derived from it.
47

48 With (5) we arrive at an equation identical to that for electronic Coulomb blockade
49 (except for the presence of z), and our further consideration follows standard Coulomb
50
51
52
53
54
55
56
57
58
59
60

Coulomb blockade model of permeation and selectivity in biological ion channels 10

blockade theory [53, 55]. Remarkably, however, the ionic version of the phenomenon exhibits valence selectivity precisely because it contains the valence z .

To interpret the conduction bands in terms of Coulomb blockade, we calculate U_n as a function of Q_f for $n = 0, 1, 2, 3$ and examine the minimum (i.e. ground state) energy

$$U_G(Q_f) = \min_n(U_n(Q_f, n)) \quad (\text{Ground state energy}) \quad (6)$$

for the ground state occupancy n_G , and the excess charge Q_G , all as functions of Q_f (see Figures 2(c) and 3(c)). The ground state (6) is by definition a stable state in thermal equilibrium.

Coulomb blockade appears in low-capacitance systems on account of quantization of the quadratic energy in (5) on a grid of discrete states (3), provided that the ground state $\{n_G\}$ is separated from neighbouring $\{n_G \pm 1\}$ states by large Coulomb energy gaps as function of geometry (R, L) and ion valence z :

$$U_s = \frac{e^2}{2C_s} = \frac{\lambda_B L}{2R^2}, \quad U_{s,z} = z^2 U_s \gg 1 \quad (\text{Coulomb gap}) \quad (7)$$

where λ_B stands for Bjerrum length [49] (0.7nm for water at $T = 298\text{K}$). This is the applicability condition for the *strong electrostatic exclusion principle*. Ion channels are extremely small and have tiny capacitance: the dimensionless self-energies of monovalent and divalent ions are $U_{s,1} \approx 5$ and $U_{s,2} \approx 20$, respectively, providing strong Coulomb blockade effects for divalent ions.

It follows from (5) that U_n vs. Q_f for given z is described by an equidistant set of identical parabolæ of period equal to the ionic charge ze . These patterns are plotted for Ca^{2+} in figure 2(c) and for Na^+ in figure 3(c). We note that $U_G(Q_f)$ exhibits two different kinds of ground state singular points, marked as M_n and Z_n . The minima of U_n (and correspondingly the blockade regions) appear around the neutralisation points $Z_n = -zen$ where the net charge at the selectivity filter $Q_n = 0$ and the occupancy P_c is saturated at an integer value [51, 58].

Figure 2(c) illustrates the fact that for Ca^{2+} the ground state $\{n_G\}$ Z_n points are separated from neighbouring $\{n_G \pm 1\}$ states by an impermeable Coulomb gap of ~ 20 (see (7)) hence providing strong Coulomb blockade. At the neutralized ($Q_n = 0$) blockade points Z_n , Ca^{2+} ions are prohibited by the self-energy barrier from entering the uncharged channel. The crossover points M_n ($U_n = U_{n+1}$) allow low-barrier (almost barrier-less) $\{n\} \rightleftharpoons \{n+1\}$ transitions (*cf.* figure 1 (b)); they correspond to the P_c transition regions and to the conduction peaks in J [58]. The M_n points are separated from higher energy states by impermeable barriers of ~ 40 ; these points are equivalent to the ion-exchange transitions reported by Zhang *et al.* [51].

The pattern of sodium ground states in figure 3(c) arises from energy gaps U_c that are $4\times$ smaller than for calcium, They are too small to prevent thermally activated transitions between neighbouring states and they allow the coexistence of more than two $\{n\}$ -states; correspondingly there is only a weak exclusion principle, in turn giving rise to weak Coulomb blockade.

The positions of the singular Q_f points in figure 2(a) can be written as:

$$\begin{aligned} Z_n &= -zen \pm \delta Z_n, & (\text{Coulomb blockade}) \\ M_n &= -ze(n + 1/2) \pm \delta M_n & (\text{Resonant conduction}) \end{aligned} \quad (8)$$

where $\delta Z_n, \delta M_n$ are possible corrections for the singular parts of the affinity and ion-ion interaction (see above) and possible electrostatic field leakage. Equations (8) describe two interleaved periodic sets of points having periods equal to the ionic charge ze , very similar to their counterparts in electronic Coulomb blockade [54].

The points $Z_n = -zen$ are neutralisation points, where the excess charge $Q_n = 0$ and U_G takes minimal values. Such points are stable and current is prohibited. Charge neutrality is important, but it is not the only factor that influences channel conductance: the term $\pm\delta Z_n$ accounts formally for the other factors (unaccounted parts of ion-ion/ion-ligand interactions and hydration energy, fields leaks etc).

The points $M_n = -ze(n + 1/2)$ are where barrier-less conduction occurs, for which $U_n = U_{n+1}$. Similarly, the terms $\pm\delta M_n$ account formally for any unconsidered perturbations.

We may therefore interpret the Brownian dynamics-simulated calcium conduction bands of figure 2(a) as Coulomb blockade conductance oscillations [55] which appear in this case as $|Q_f|$ is being increased, and the corresponding occupancy steps in figure 2(b) as a Coulomb staircase [56]. The deviations in the precise positions of M_n and Z_n can be attributed to field leaks and the model simplifications.

3.3. Identification of bands with real calcium channels

Table 1, showing the putative identifications of the bands/singularities in the Coulomb blockade model with real channels, wild type and mutants in the $\text{Ca}^{2+}/\text{Na}^+$ family, has been extended from [57, 58].

Table 1(a) describes shows identifications of conduction bands with wild type channels.

The single-ion Na^+ barrier-less point L_0 can be speculatively identified with the non-selective DEKA sodium channel ($Q_f = -1e$) [1, 17]. The single-ion Ca^{2+} barrier-less point M_0 can be identified with the non-selective OmpF porin ($Q_f = -1e$) [27], or with nonselective Na^+ -K channel [81].

Mammalian calcium channels exist in several modifications. Some of them (L-type, T-type) share the same highly-conserved 4-glutamate (EEEE) locus at the selectivity filter with nominal $Q_f = -4e$ [14]. The permeation properties (sharp selectivity, AMFE, double-ion nature of calcium permeation) of these channels are consistent with the double-ion $M_1 \text{Ca}^{2+}$ conduction band [57, 58]. Double-ion knock-on mechanism of conduction and selectivity of L-type calcium channel has been derived from experimentally observed double-affinity of AMFE [14, 78]. The same M_1 peak can be also identified with the Ca^{2+} -selective mutant of the Nav sodium channel ($Q_f = -3e$) [22] and a calcium-selective mutant of OmpF porin ($Q_f = -4e$) [27].

Table 1. Putative identification of ionic Coulomb blockade model bands with some known wild type (WT) channels and mutants sequences (extended from [58]).

N	Channel/mutant	Site locus	Nom. Q_f/e	Band	Band's Q_f/e
(a)	WT Na ⁺ -selective Nav channel [22]	DEKA	-1	L ₀	-0.5
	WT Non-selective OmpF [27]	KRRRDE	-1	M ₀	-1
	WT Ca ²⁺ -selective L-type channel [23]	EEEE	-4	M ₁	-3
	WT NaChBac[18], NavAB [28]	EEEE	-4	Z ₂	-4
	WT Ca ²⁺ -selective RyR channel [7]	DDDD(ED)	-6	M ₂	-5
(b)	WT Na ⁺ -selective Nav channel [22]	DEKA	-1	L ₀	-0.5
	Ca ²⁺ -blocked Nav mutant	⇒ DEKE	-2	M ₀	-1
	Ca ²⁺ -permeable Nav mutant	⇒ DEEA	-3	Z ₁	-2
	Ca ²⁺ -selective Nav mutant	⇒ EEEE	-4	M ₁	-3
(c)	WT Ca ²⁺ -selective L-type channel [23]	EEEE	-4	M ₁	-3
	Ca ²⁺ -blocked Cav mutant	⇒ EEQE	-3	Z ₁	-2
	Na ⁺ -conductive Cav mutant	⇒ EEKE	-2	M ₀	-1
	Na ⁺ -selective Cav mutant	⇒ EEKA	-1	L ₀	-0.5
(d)	WT Na ⁺ -selective NaChBac[18]	EEEE	-4	Z ₂	-4
	Ca ²⁺ -selective CaChBac mutant	⇒ EEEE+DDDD	-7	M ₃	-8
(e)	WT Na ⁺ -selective NavAB[28]	EEEE	-4	Z ₂	-4
	Ca ²⁺ -selective CavAB mutant	⇒ EEEE+DDDD	-7	M ₃	-8

The Ryanodine receptor RyR calcium channel has $Q_f \approx -6e$ and relatively weak selectivity [7]. We connect it with $M_2 \approx -5e$ three-ion conduction point [57, 58].

Bacterial sodium channels, NaChBac [18] and NavAB [28] possess EEEE loci (with nominal $Q_f = -4e$), typical of mammalian calcium channels but nonetheless exhibit Na⁺-selective features and divalent blockade. We connect them (speculatively) with the Z₂ Ca²⁺ blockade point for $Q_f = -4e$.

It is evident that the nominal charges of the channel loci exceed the charge of the model bands by nearly $\Delta Q_f = 1e$. For example, at M₁ we have $Q_f = -3e$ from the Coulomb blockade model, whereas the nominal $Q_f = -4e$ for the EEEE loci of L-type calcium channels (and there are corresponding discrepancies at the M₂ and M₃ points). We speculate that these systematic discrepancies may be connected to field leaks, to the distant influence of the positive charges of the other ends of the amino acids buried in the rest of the protein, or to possible protonation of the side chains [82]. Molecular dynamics simulations [28, 35, 38] could be particularly helpful in determining the effective values of Q_f for wild type and mutant channels.

The above identification scheme can thus account for many mutation transformations observed in the Ca²⁺/Na⁺ channels family. The main test and validation of the Coulomb blockade model is the correct prediction that single $\pm 1e$ mutations should lead to sharp changes of calcium conductance from resonance to blockade and *vice versa*.

Similarly, table 1(b) describes the radical mutation-induced transformation of the Nav sodium channel to a calcium channel, when the DEKA locus has been sequentially changed by point mutations [22].

Table 1(c) shows that the downward mutations of EEEE calcium channels described in [23] lead to a moderate decrease of divalent/monovalent ($\text{Ba}^{2+}/\text{Na}^{+}$) selectivity for EEEE(-4e)→EQEE (-3e) mutation and a sharp, two-order decrease for the EEEE(-4e)→EKEE (-2e) mutation (though see discussion below).

Table 1(d),(e) show that the upward mutations of the EEEE loci of bacterial sodium channels (EEEE (-4e) ⇒ EEEE+DDDD (-8e)) calcium channels described in [18, 28] lead to channel transformation to a calcium-selective mutant CaChBac and CavAB, respectively. Ca^{2+} selective mutants demonstrate selectivities of up to $600\times$ in favour of Ca^{2+} ions over Na^{+} , and AMFE. We putatively connect these transformations with the jump $Z_2 \Rightarrow M_3$. Note, that the model predicts rather high numbers of ions inside the channel (between 3 and 4 for M_3) but there is no experimental evidence to support these specific occupancy numbers.

One of the most striking consequences of the Coulomb blockade oscillations is that, for channels having $Q_f \approx M_n$, adding one negative charge should dramatically *decrease* the Ca^{2+} conductance. So far, all mutation chains showed increase of calcium selectivity with growth of negative Q_f which can also, however, be explained by alternative models [32]. On the other hand these experiments are limited to $|Q_f| \leq 4e$ where the Coulomb blockade model also predicts an experimental increase of calcium selectivity with growth of $|Q_f|$ in the range $|Q_f| = 0 - 4e$ (see Fig. 11 of [58]) but predicts a sharp drop in calcium selectivity near the neutralisation blockade point Z_2 .

We can suppose that the NavAB/NaChBac EEEE locus has an effective $Q_f = Z_2 = -4e$, and hence a $1e$ mutation of the EEEE ring (or a $\pm 1e$ mutation of the neighbouring ring of residues) should lead to increase of S for both directions of mutation. The currently available data (see Table (d),(e)) were obtained for mutation steps of $Q_s = 4e$ and thus cannot resolve the effect of the smaller $1e$ jumps.

These identifications can be seen as an initial verification of the Coulomb blockade model predictions, albeit with some discrepancies. Further investigations are needed to confirm the channel identifications, to understand why the nominal Q_f is systematically slightly smaller than the Q_f values of band maxima in the model, and to establish the reason why mammalian and bacterial channels with EEEE-loci have opposite selectivity properties.

3.4. Shapes of the Coulomb blockade oscillations

We now develop a description of the (interconnected) shapes of the Coulomb blockade oscillations in J , and the Coulomb staircase in P . We consider the case of divalent Ca^{2+} bands arising from strong Coulomb blockade (figure 2).

The equilibrium distribution of P_c in the vicinity of the M_n points (and hence calculation of the shapes of $P_c(U)$ or $P_c(Q_f)$) follows from standard Coulomb blockade

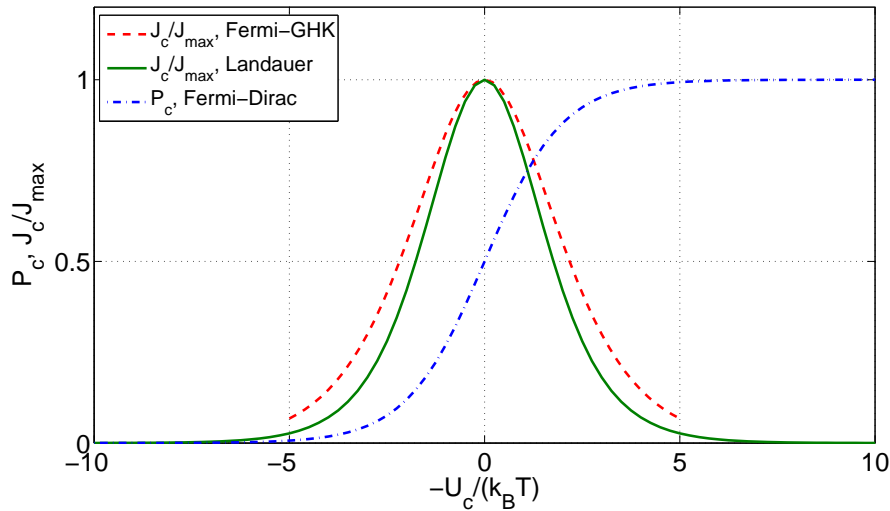


Figure 4. The calculated occupancy P and current J as U_c (or equivalently Q_f) is varied. The occupancy P_c (blue, dash-dot) shows the Fermi-Dirac transition from $P_c = 0$ to $P_c = 1$. The currents calculated in the Landauer $J_c \sim dP/dU$ (green, solid) and Fermi-GHK (red, dashed) approximations both exhibit resonant peaks in the transition region.

theory. As mentioned above, the energy level separation for divalent Ca^{2+} is so large (≈ 40) that the general set of eigenstates (3) reduces to a simple 2-state exclusive set:

$$m = \{n, n + 1\}; \quad \theta_n + \theta_{n+1} = 1; \quad P_c = n + \theta_{n+1}. \quad (9)$$

The electrostatic exclusion principle (9) plays the same role here as that of the Pauli exclusion principle in quantum mechanics [83–85]; the standard derivation via the partition function, taking account of exclusion principle (9) leads [86–88] to Fermi-Dirac statistics for θ_{n+1} and an excess (fractional) occupancy $P_c^* = P_c \bmod 1$:

$$P_c^* = (1 + \exp(U_{n+1} - \mu))^{-1} = (1 + P_b^{-1} \exp(U_c))^{-1}, \quad (10)$$

where $\mu = \mu_0 + \ln P_b$ is the chemical potential, P_b is a reference occupancy related to the bulk concentration, and μ_0 is a constant potential assumed here to be $\mu_0 = \langle U \rangle = (U_n + U_{n+1})/2$. Hence:

$$U_c = U_{n+1} - \mu_0 = (U_{n+1} - U_n)/2. \quad (11)$$

The Fermi-Dirac equation (10) is equivalent to the Langmuir isotherm [86] and to Michaelis-Menten saturation. A similar Fermi function was obtained earlier [51] for the variation of P_c with concentration.

Note that the Fermi-Dirac distribution needed for cases where the exclusion principle is based on volume exclusion, and the ions have unequal diameters, has been investigated by Liu and Eisenberg [85, 89, 90].

It follows from (5) that U_c is a linear function of Q_f :

$$U_c = k_z \frac{\Delta Q_f}{e}, \quad (12)$$

Coulomb blockade model of permeation and selectivity in biological ion channels 15

where $\Delta Q_f = Q_f - M_n$ and $k_z = zU_s$. Hence the Fermi-Dirac function (10) also describes the dependence of P^* on Q_f :

$$P_c^* = \left(1 + P_b^{-1} \exp \left(k_z \frac{\Delta Q_f}{e} \right) \right)^{-1}, \quad (13)$$

where for our geometry with for $z = 2$ (Ca^{2+} ions) the dimensionless scaling coefficient $k_z \approx 10$. This is the final result for the shape of the Coulomb staircase of occupancy *vs.* as a function of Q_f . Fig. 2(b) shows qualitative agreement of $P(Q_f)$ shapes with (13), including the concentration-dependent shift between curves with different P_b . We will make a more detailed comparison below.

Approximate forms of the current as a function of energy (or fixed charge) can be found via the variance σ of the Fermi-Dirac occupancy P due to thermal fluctuations, as follows from the fluctuation-dissipation theorem and linear response theory [91]. The ability of an energy level to contribute to the current/conductance is then proportional to $\sigma^2 = dP/dU_c$ via the Landauer approximation [54, 55]:

$$\frac{J_c}{J_{max}} \propto \frac{dP}{dU_c} = \cosh^{-2} \left(\frac{U_c}{2} \right), \quad (14)$$

where J_{max} is the barrier-less diffusive current. Taking account of scattering, one reaches the standard Coulomb blockade theory approximation [55, 92]:

$$\frac{J_c}{J_{max}} = U_c \sinh^{-1} (U_c) \approx \cosh^{-2} \left(\frac{U_c}{2.5} \right) \quad (15)$$

Alternatively (15) can be derived by the quasi-equilibrium (or nonequilibrium reaction rate [93]) approach with explicit solution of the Nernst-Planck equation (i.e. the Goldman-Hodgkin-Katz (GHK) solution) taking account of the Fermi-Dirac occupancy (10), so (15) can thus be called the Fermi-GHK approximation; a similar result was obtained earlier by Mott [94, 95].

Figure 4 reveals a resonant conductivity as U_c is varied, for both the Landauer (14) and Fermi-GHK (15) approximations: in each case there is a peak coinciding with the maximum in the derivative of P_c , dP/dU_c . (Note that, from (5), variation of U_c is equivalent to variation of Q_f .) In practical terms, the difference between the two approximations is small: they both represent double-exponential peaks of half-width $U_{1/2} \approx 2.3$. The form of this current is similar to that of the tunneling current in a quantum dot [54]: an even, double-exponential function of U_c , reflecting the symmetry of the escape and relaxation trajectories [96]. Note that even small asymmetries, easy to overlook, can have disquieting effects [97].

For a quantitative comparison of the theory with P_c as obtained from the Brownian dynamics simulations, we calculate the effective (excess) well depth U_c^* as:

$$U_c^* = \ln \frac{1 - P_c^*}{P_c^*} = k_z \frac{\Delta Q_f}{e} \quad (16)$$

The Fermi-Dirac function (10) predicts that U_c^* should be linear in Q_f , i.e. (16) represents linearising coordinates for the Fermi-Dirac equation (10); the Coulomb blockade model also predicts the geometry-dependent coefficient k_z .

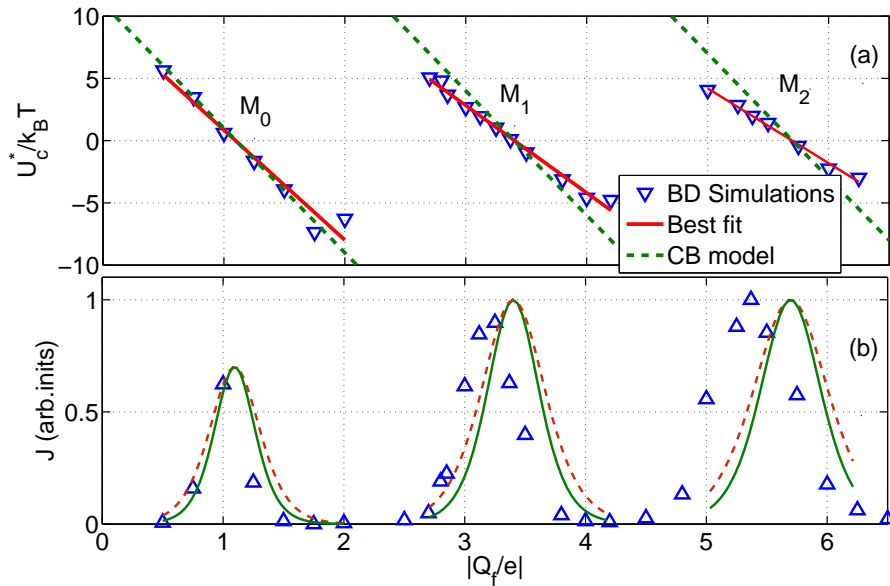


Figure 5. Comparisons of the ionic Coulomb blockade model with Brownian dynamics (BD) simulation results as Q_f is varied. (a) The effective well depth U_c^* (blue point-down triangles) fitted by Fermi-Dirac function (16) with best-fit slopes (full red lines) and with analytical slopes k_z (green dashed lines). (b) The full green curves representing the Landauer approximation (14), and the red-dashed lines representing the Fermi-GHK approximation (15), are compared with the Brownian dynamics simulations (blue, point-up triangles)..

Figure 5(a) shows a sawtooth-like dependence of U_c^* on Q_f , confirming that the P_c^* transitions obey the Fermi-Dirac function (10) of U_c . For M_1 , the slope corresponds well with analytic k_z ; the discrepancies in slope at M_2 and M_3 are attributable to our neglect of ion-ion interactions.

Figure 5(b) compares the predictions of the Coulomb blockade model with the conduction bands M_0 , M_1 , M_2 obtained from the simulations [57]. The Landauer and Fermi-GHK peaks are calculated using (14) and (15) respectively with the values of U_c^* taken from plot (a), and there are no adjustable parameters. The BD peak shapes and positions are described reasonably well by the model, extending the simpler fitting in [58, 59]. Again, the agreement is very good for M_1 , and less good for M_2 and M_3 on account of our neglect of field leaks and the singular parts of the interactions.

In general, the results of Brownian dynamics simulations [57, 58] correspond well with the predictions of the Coulomb blockade model.

3.5. Valence selectivity and AMFE

Comparison of the Ca^{2+} ($z = 2$) bands pattern (figure 2) with the Na^+ ($z = 1$) picture (figure 3) clearly shows that, unlike its electronic counterpart, ionic Coulomb blockade is valence-dependent: the positions of the bands $M_0 = ze/2$, and their period ze , shift in proportion to z as described by equation (8) and they broaden/narrow in proportion

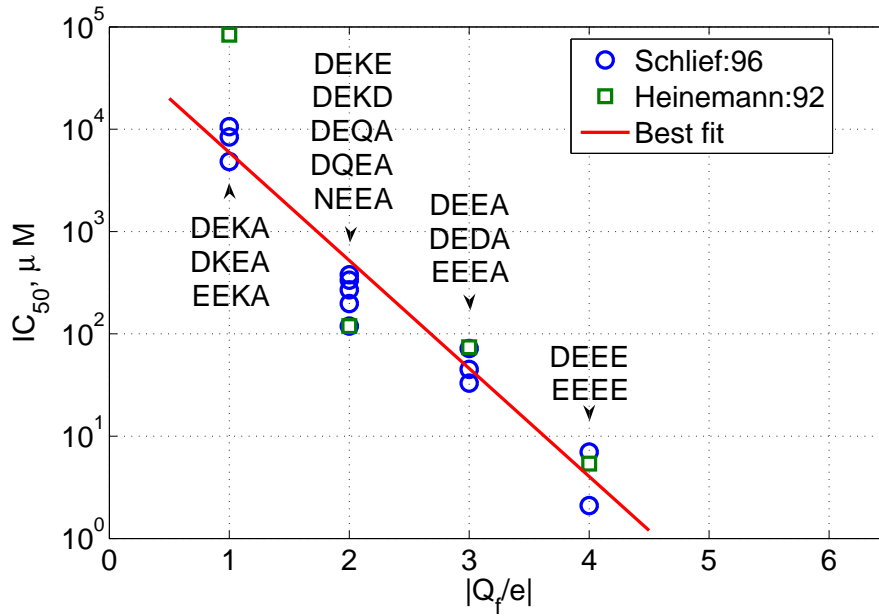


Figure 6. Calcium block as a function of the net charge Q_f of the sodium channel inner ring mutants (relative to the wild type (DEKA)). For the indicated mutants IC_{50} (i.e. the concentration $[Ca^{2+}]$ necessary to block 50% of sodium inward current) is plotted as a function of the net charge of the inner ring Q_f . Data points are taken from [24] (blue open circles) and [22] (green open squares). The continuous red line indicates an exponential function $a \exp(-b|Q_f/e|)$, with $b = 2.29$, corresponding to a least-squares fit to all the data.

to z^2 (5) [58].

The ionic Coulomb blockade model attributes selectivity to modification of the U_G dependences on Q_f . Valence selectivity is provided by the electrostatic z -dependent shift of $U_G(n, Q_f)$ curves and the corresponding shifts of the M_n and Z_n singular points. Alike-charge selectivity can in principle be accounted by hydration-dependent shifts of M_n and Z_n .

The model also predicts that a monovalent (e.g. sodium) ionic current can be effectively blocked by a few divalent (e.g. calcium) ions, an effect well-known in calcium and sodium channels. Calcium blockade is an aspect of AMFE, which is a signature of EEEE calcium channels [14]. The threshold of the divalent block IC_{50} is defined as the Ca^{2+} concentration which results in a 50% decrease in the monovalent current [14]. We can estimate IC_{50} on the assumption that the sodium current is proportional to $(1 - P_{Ca})$, i.e. to the fraction of time when the channel is not blocked by calcium ions. Hence equations (12, 13) result in an exponential dependence of IC_{50} on Q_f :

$$IC_{50} \propto \exp\left(k_2 \frac{\Delta Q_f}{e}\right), \quad (17)$$

which is a prediction that can be tested.

Mutant studies of the DEKA sodium channel [22, 24, 26] have measured the dependence of AMFE on the selectivity filter locus and its Q_f , and it was shown that

1
2
3 *Coulomb blockade model of permeation and selectivity in biological ion channels* 18

4
5 $\log(IC_{50})$ can successfully be fitted by a linear function of Q_f (figure 6), in agreement
6 with the prediction (17) of the Coulomb blockade model, or

$$7 \quad \log(IC_{50}) = a + b \frac{Q_f}{e}, \quad (18)$$

10 where a and b are constants. The best-fit line gives $b = 2.29$ [24] which does not agree
11 well with the $b = k_2 \approx 10$ calculated for our model. This discrepancy can be interpreted
12 as evidence that the geometrical parameters (R and L) of the selectivity filter of a DEKA
13 sodium channel differ from values taken in our model ($R = 0.3\text{nm}$, $L = 1.6\text{nm}$). To
14 be compatible with experiments the selectivity filter would need to be shorter and/or
15 wider. We can get good agreement for e.g. $R = 3.5\text{nm}$ and $L = 0.4\text{nm}$ (such a short
16 selectivity filter would in fact correspond well to the model of [70]) for which $k_2 = 2.28$.
17 Because the exact values are not yet known, our fitting can be used to estimate these
18 parameters. **Note, however, that the fitting (18) is not unique to the Coulomb blockade
19 model but follows from the dominance of electrostatics for divalent ions [24].**

24 3.6. Further considerations

25
26 Although an ion moving inside a channel is a room-temperature classical system
27 described by Newtonian dynamics, we see that it exhibits some quantum-like mesoscopic
28 features [52]. They include the appearance of strong Coulomb blockade oscillations in
29 conductance, a Coulomb staircase, and a Fermi-Dirac distribution of occupancy for Ca^{2+}
30 ions. We attribute such behavior to the charge discreteness, to the strong electrostatic
31 interaction in confinement [52] and to the electrostatic exclusion principle. It has been
32 shown rigorously that, in the presence of an exclusion principle, Brownian motion leads
33 to a Fermi-Dirac distribution of the Brownian particles [84].

34 A parametric study [57] based on Brownian dynamics modelling has shown that,
35 in accordance with (7), strong Coulomb blockade may be expected in channels of radii
36 $R = 0.25 - 0.35\text{nm}$ for ions having $z = 2$, e.g. for Ca^+ ions in calcium/sodium channels.
37 It is an interesting and significant question whether or not strong blockade and the
38 corresponding oscillations may also arise in the conduction of monovalent ions in K^+
39 channels. The latter have a selectivity filter of appropriate radius, $R \approx 0.25\text{nm}$ [34].
40 Furthermore, K^+ ions are fully hydrated, which should lead to a stronger electrostatic
41 interaction and hence to a marked decrease in the effective ε_w , bringing it close to
42 $\varepsilon_w = 1$. In such a case equation (7) suggests that we could expect an observable
43 Coulomb blockade effect, even for monovalent ions in potassium channels [40, 41], a
44 speculation that needs to be tested.

45 The relationship of the stop bands in the model to the subconductance states
46 seen in experiments, and to the noise of closed channels, remains to be determined.
47 Subconductance states and unusual baseline noise are found in a wide variety of natural
48 biological channels [98].

1
2
3
4
5
6
7
8
9
10
11
12
13
14
15
16
17
18
19
20
21
22
23
24
25
26
27
28
29
30
31
32
33
34
35
36
37
38
39
40
41
42
43
44
45
46
47
48
49
50
51
52
53
54
55
56
57
58
59
60

4. Conclusions

We conclude that ionic Coulomb blockade manifests itself in a simple electrostatic and Brownian dynamics model of a water-filled charged nanopore with parameters chosen to correspond to those of biological ion channels. It is a fundamental electrostatic phenomenon based on charge discreteness, an electrostatic exclusion principle and linear response theory. For divalent Ca^{2+} ions in calcium/sodium channels, the blockade is strong, so that the ionic permeation process is closely analogous to low-temperature mesoscopic transport in quantum dots. The several similarities include the applicability of Fermi-Dirac statistics and the appearance of Coulomb blockade oscillations, i.e. the calcium ion channel can behave as a single-charge discrete electrostatic device.

For the parameter range where it is applicable and strong, the ionic Coulomb blockade picture leads to several explicit predictions that are unique to the model:

- Periodic oscillations of conductance *vs.* Q_f with a period close to the ionic charge ze , with stop-bands Z_n centred on positions $-zen$, and conduction-bands M_n centred on $-ze(n + 1/2)$.
- Hence, a valence dependence of the pattern of bands, leading to valence selectivity.
- Fermi-Dirac occupancy statistics and corresponding shapes of the occupancy bands.
- The barrier-less character of conduction at the M_n points.

The approach also provides straightforward (**provisional**) explanations of many experimentally observed phenomena in the $\text{Ca}^{2+}/\text{Na}^+$ channels family including:

- Fast permeation, which can be accounted for through barrier-less single- and multi-ion conductivity.
- The strong valence selectivity of calcium channels.
- Divalent block of a monovalent current and the anomalous mole-fraction effect (AMFE).
- The mutation transformations of conduction and selectivity.

The ionic Coulomb blockade model of ionic permeation provides a simple and transparent explanation of a wide range of experimental data that hitherto had not seemed to be connected, and it reinterprets the calcium conduction bands as manifestations of a quite general electrostatic phenomenon, common to ion channels, quantum-dots, and tunnel diodes.

Currently available experimental data do not allow for full validation of the Coulomb blockade model and, moreover, there are some small discrepancies. Therefore, we present this theory as something still awaiting full verification through comparison with experimental results from real biological channels, rather than as something already “verified”. Further investigations are needed to confirm/refute the tentative channel identifications, to understand why the nominal Q_f is systematically slightly smaller than the Q_f values of band maxima in the model, and to explain why mammalian and bacterial EEEE-loci channels have different selectivity properties.

Finally, we remark that the results could also be applicable to other ion channels and to biomimetic nanopores with charged walls.

Coulomb blockade model of permeation and selectivity in biological ion channels 20

Acknowledgements

We acknowledge valuable discussions with Mark Dykman, Will Gibby, Dmitrii Luchinsky, Aneta Stefanovska and Rodrigue Tindjong. Igor Kaufman is also grateful to Boris Shklovskii and Max Di Ventra for helpful comments and discussions. The research was supported by the Engineering and Physical Sciences Research Council UK (grants Nos. EP/G070660/1 and EP/M015831/1).

References

- [1] Hille, B., *Ion Channels Of Excitable Membranes* (Sinauer Associates, Sunderland, MA, 2001), 3rd edn.
- [2] Ashcroft, F. M., From molecule to malady, *Nature* **440**, 440–447 (2006).
- [3] Eisenberg, B., Ionic interactions are everywhere, *Physiol.* **28**, 28–38 (2013).
- [4] Rubaiy, H. N. & Linsdell, P., Location of a permeant anion binding site in the cystic fibrosis transmembrane conductance regulator chloride channel pore, *J. Physiol. Sci.* DOI 10.1007/s12576-015-0359-6 (2015).
- [5] Eisenman, G. & Horn, R., Ionic selectivity revisited: the role of kinetic and equilibrium processes in ion permeation through channels, *J. Membrane Biol.* **76**, 197–225 (1983).
- [6] Laio, A. & Torre, V., Physical origin of selectivity in ionic channels of biological membranes, *Biophys. J.* **76**, 129–148 (1999).
- [7] Gillespie, D., Energetics of divalent selectivity in a calcium channel: The ryanodine receptor case study, *Biophys. J.* **94**, 1169–1184 (2008).
- [8] Zwolak, M., Lagerqvist, J. & Di Ventra, M., Quantized ionic conductance in nanopores, *Phys. Rev. Lett.* **103**, 128102 (2009).
- [9] Krauss, D., Eisenberg, B. & Gillespie, D., Selectivity sequences in a model calcium channel: role of electrostatic field strength, *Eur. Biophys. J.* **40**, 775–782 (2011).
- [10] Eisenberg, B. & Liu, W., Poisson-Nernst-Planck systems for ion channels with permanent charges, *SIAM J. Math. Anal.* **38**, 1932–1966 (2007).
- [11] Abaid, N., Eisenberg, R. S. & Liu, W., Expansions of I-V relations via a Poisson-Nernst-Planck system, *SIAM J. Appl. Dyn. Syst.* **7**, 1507–1526 (2008).
- [12] Ji, S. & Liu, W., Poisson-Nernst-Planck systems for ion flow with density functional theory for hard-sphere potential: I-V relations and critical potentials. Part I: Analysis, *J. Dyn. Diff. Eq.* **24**, 955–983 (2012).
- [13] Liu, W., Tu, X. & Zhang, M., Poisson-Nernst-Planck systems for ion flow with density functional theory for hard-sphere potential: I-V relations and critical potentials. Part II: Numerics, *J. Dyn. Diff. Eq.* **24**, 985–1004 (2012).
- [14] Sather, W. A. & McCleskey, E. W., Permeation and selectivity in calcium channels, *Ann. Rev. Physiol.* **65**, 133–159 (2003).
- [15] Corry, B., Allen, T. W., Kuyucak, S. & Chung, S. H., Mechanisms of permeation and selectivity in calcium channels, *Biophys. J.* **80**, 195–214 (2001).
- [16] Giri, J., Fonseca, J. E., Boda, D., Henderson, D. & Eisenberg, B., Self-organized models of selectivity in calcium channels, *Phys. Biol.* **8**, 026004 (2011).
- [17] Catterall, W. A., Voltage-gated sodium channels at 60: structure, function and pathophysiology, *J. Physiol.* **590**, 2577–2589 (2012).
- [18] Yue, L. X., Navarro, B., Ren, D. J., Ramos, A. & Clapham, D. E., The cation selectivity filter of the bacterial sodium channel, NaChBac, *J. Gen. Physiol.* **120**, 845–853 (2002).
- [19] Payandeh, J., Scheuer, T., Zheng, N. & Catterall, W. A., The crystal structure of a voltage-gated sodium channel, *Nature* **475**, 353–358 (2011).

- 1
2
3 *Coulomb blockade model of permeation and selectivity in biological ion channels* 21
4
- 5 [20] Corry, B., Na⁺/Ca²⁺ selectivity in the bacterial voltage-gated sodium channel NavAb, *PeerJ* **1**,
6 e16 (DOI10.7717/peerj.16) (2013).
- 7 [21] Sakmann, B. & Neher, E. (eds.), *Single-Channel Recording* (Springer, Berlin, 2009).
- 8 [22] Heinemann, S. H., Teriau, H., Stuhmer, W., Imoto, K. & Numa, S., Calcium-channel characteristics
9 conferred on the sodium-channel by single mutations, *Nature* **356**, 441–443 (1992).
- 10 [23] Tang, S. Q., Mikala, G., Bahinski, A., Yatani, A., Varadi, G. & Schwartz, A., Molecular localization
11 of ion selectivity sites within the pore of a human L-type cardiac calcium channel, *J. Biol. Chem.*
12 **268**, 13026–13029 (1993).
- 13 [24] Schlieff, T., Schonherr, R., Imoto, K. & Heinemann, S. H., Pore properties of rat brain II sodium
14 channels mutated in the selectivity filter domain, *Eur. Biophys. J.* **25**, 75–91 (1996).
- 15 [25] Favre, I., Moczydlowski, E. & Schild, L., On the structural basis for ionic selectivity among Na⁺,
16 K⁺, and Ca²⁺ in the voltage-gated sodium channel, *Biophys. J.* **71**, 3110–3125 (1996).
- 17 [26] Sun, Y. M., Favre, I., Schild, L. & Moczydlowski, E., On the structural basis for size-selective
18 permeation of organic cations through the voltage-gated sodium channel – Effect of alanine
19 mutations at the DEKA locus on selectivity, inhibition by Ca²⁺ and H⁺, and molecular sieving,
20 *J. Gen. Physiol.* **110**, 693–715 (1997).
- 21 [27] Miedema, H., Meter-Arkema, A., Wierenga, J., Tang, J., Eisenberg, B., Nonner, W., Hektor, H.,
22 Gillespie, D. & Meijberg, W., Permeation properties of an engineered bacterial OmpF porin
23 containing the EEEE-locus of Ca²⁺ channels, *Biophys. J.* **87**, 3137–3147 (2004).
- 24 [28] Tang, L., El-Din, T. M. G., Payandeh, J., Martinez, G. Q., Heard, T. M., Scheuer, T., Zheng,
25 N. & Catterall, W. A., Structural basis for Ca²⁺ selectivity of a voltage-gated calcium channel,
26 *Nature* **505**, 56–61 (2014).
- 27 [29] DeCaen, P. G., Takahashi, Y., Krulwich, T. A., Ito, M. & Clapham, D. E., Ionic selectivity and
28 thermal adaptations within the voltage-gated sodium channel family of alkaliphilic Bacillus,
29 *eLife* **3**, e04387 (2014).
- 30 [30] Corry, B., Vora, T. & Chung, S. H., Electrostatic basis of valence selectivity in cationic channels,
31 *Biochim. Biophys. Acta-Biomembranes* **1711**, 72–86 (2005).
- 32 [31] Boda, D., Nonner, W., Henderson, D., Eisenberg, B. & Gillespie, D., Volume exclusion in calcium
33 selective channels, *Biophys. J.* **94**, 3486–3496 (2008).
- 34 [32] Csányi, E., Boda, D., Gillespie, D. & Kristf, T., Current and selectivity in a model sodium
35 channel under physiological conditions: Dynamic Monte Carlo simulations, *Biochim. Biophys.*
36 *Acta (BBA) – Biomembranes* **1818**, 592–600 (2012).
- 37 [33] Dudev, T. & Lim, C., Evolution of eukaryotic ion channels: Principles underlying the conversion
38 of Ca²⁺-selective to Na⁺-selective channels, *J. Amer. Chem. Soc.* **136**, 3553–3559 (2014).
- 39 [34] Doyle, D. A., Cabral, J. M., Pfuetzner, R. A., Kuo, A., Gulbis, J. M., Cohen, S. L., Chait, B. T.
40 & MacKinnon, R., The structure of the potassium channel: Molecular basis of K⁺ conduction
41 and selectivity, *Science* **280**, 69–77 (1998).
- 42 [35] Roux, B., Allen, T., Berneche, S. & Im, W., Theoretical and computational models of biological
43 ion channels, *Quart. Rev. Biophys.* **37**, 15–103 (2004).
- 44 [36] Brooks, B. R. *et al.*, CHARMM: The biomolecular simulation program, *J. Comp. Chem.* **30**,
45 1545–1614 (2009).
- 46 [37] Berneche, S. & Roux, B., Energetics of ion conduction through the K⁺ channel, *Nature* **414**, 73–77
47 (2001).
- 48 [38] Jensen, M. Ø., Jogini, V., Borhani, D. W., Leffler, A. E., Dror, R. O. & Shaw, D. E., Mechanism
49 of voltage gating in potassium channels, *Science* **336**, 229–233 (2012).
- 50 [39] Shaw, D. E. & *et al*, Anton 2: raising the bar for performance and programmability in a special-
51 purpose molecular dynamics supercomputer, in *Proceedings of the International Conference*
52 *for High Performance Computing, Networking, Storage and Analysis*, 41–53 (IEEE Press,
53 Piscataway, 2014).
- 54 [40] Köpfer, D. A., Song, C., Gruene, T., Sheldrick, G. M., Zachariae, U. & de Groot, B. L., Ion
55 permeation in K⁺ channels occurs by direct Coulomb knock-on, *Science* **346**, 352–355 (2014).
- 56
57
58
59
60

- 1
2
3 *Coulomb blockade model of permeation and selectivity in biological ion channels* 22
4
5 [41] Hummer, G., Potassium ions line up, *Science* **346**, 303–303 (2014).
6 [42] Eisenberg, R., Ion channels, natural nanovalves, in G. Kreysa, K. Ota & R. F. Savinell (eds.),
7 *Encyclopedia of Applied Electrochemistry*, 1089–1093 (Springer, 2014).
8 [43] Hoyles, M., Kuyucak, S. & Chung, S.-H., Computer simulation of ion conductance in membrane
9 channels, *Phys. Rev. E* **58**, 3654–3661 (1998), pRE.
10 [44] Im, W. & Roux, B., Ion permeation and selectivity of OmpF porin: a theoretical study based on
11 molecular dynamics, Brownian dynamics, and continuum electrodiffusion theory, *J. Mol. Biol.*
12 **322**, 851–869 (2002).
13 [45] Berti, C., Furini, S., Gillespie, D., Boda, D., Eisenberg, R. S., Sangiorgi, E. & Fiegna, C., Three-
14 dimensional Brownian dynamics simulator for the study of ion permeation through membrane
15 pores, *J. Chem. Theor. Comp.* dx.doi.org/10.1021/ct4011008 (2014).
16 [46] Eisenberg, B., Proteins, channels and crowded ions, *Biophys. Chem.* **100**, 507–517 (2002).
17 [47] Stopa, M., Rectifying behavior in Coulomb blockades: charging rectifiers, *Phys. Rev. Lett.* **88**,
18 146802 (2002).
19 [48] Millar, C., Asenov, A. & Roy, S., Self-consistent particle simulation of ion channels, *J. Comp.*
20 *Theor. Nanosci.* **2**, 56–67 (2005).
21 [49] Zhang, J., Kamenev, A. & Shklovskii, B. I., Conductance of ion channels and nanopores with
22 charged walls: A toy model, *Phys. Rev. Lett.* **95**, 148101 (2005).
23 [50] Kamenev, A., Zhang, J., Larkin, A. I. & Shklovskii, B. I., Transport in one-dimensional Coulomb
24 gases: From ion channels to nanopores, *Physica A* **359**, 129–161 (2006).
25 [51] Zhang, J., Kamenev, A. & Shklovskii, B. I., Ion exchange phase transitions in water-filled channels
26 with charged walls, *Phys. Rev. E* **73**, 051205 (2006).
27 [52] Krems, M. & Di Ventra, M., Ionic Coulomb blockade in nanopores, *J. Phys. Condens. Matter* **25**,
28 065101 (2013).
29 [53] Averin, D. V. & Likharev, K. K., Coulomb blockade of single-electron tunneling, and coherent
30 oscillations in small tunnel junctions, *J. Low Temp. Phys.* **62**, 345–373 (1986).
31 [54] Alhassid, Y., Statistical theory of quantum dots, *Rev. Mod. Phys.* **72**, 895–968 (2000).
32 [55] Beenakker, C. W. J., Theory of Coulomb-blockade oscillations in the conductance of a quantum
33 dot, *Phys. Rev. B* **44**, 1646–1656 (1991).
34 [56] Likharev, K. K., SET: Coulomb blockade devices, *Nano et Micro Tech.* **3**, 71–114 (2003).
35 [57] Kaufman, I. K., Luchinsky, D. G., Tindjong, R., McClintock, P. V. E. & Eisenberg, R. S., Multi-ion
36 conduction bands in a simple model of calcium ion channels, *Phys. Biol.* **10**, 026007 (2013).
37 [58] Kaufman, I. K., Luchinsky, D. G., Tindjong, R., McClintock, P. V. E. & Eisenberg, R. S.,
38 Energetics of discrete selectivity bands and mutation-induced transitions in the calcium-sodium
39 ion channels family, *Phys. Rev. E* **88**, 052712 (2013).
40 [59] Kaufman, I. K., Tindjong, R., Luchinsky, D. G., McClintock, P. V. E. & Eisenberg, R. S., Resonant
41 multi-ion conduction in a simple model of calcium channels, in J. M. Routoure, L. Varani &
42 F. Pascal (eds.), *22nd Intern. Conf. on Noise and Fluctuations (ICNF)*, Montpellier, 24–28 June
43 2013, doi: 10.1109/ICNF.2013.6578926 (IEEE Conf. Proc., 2013).
44 [60] Eisenberg, R. S., Computing the field in proteins and channels, *J. Membrane Biol.* **150**, 1–25
45 (1996).
46 [61] Eisenberg, R. S., Atomic biology, electrostatics and ionic channels, in R. Elber (ed.), *New*
47 *Developments in Theoretical Studies of Proteins*, 269–357 (World Scientific, Singapore, 1996).
48 [62] Catterall, W. A., Voltage-gated sodium channels: Structure, function, and molecular
49 pharmacology, in *Ion Channel Drug Discovery*, *RSC Drug Discovery Series*, vol. 39, 83–104
50 (Royal Society of Chemistry, Cambridge, 2015).
51 [63] Hu, H., Wang, Z., Wei, R., Fan, G., Wang, Q., Zhang, K. & Yin, C.-C., The molecular architecture
52 of dihydropyridine receptor/L-type Ca²⁺ channel complex, *Sci. Rep.* **5**, 8370 (2015).
53 [64] Boda, D., Henderson, D. & Gillespie, D., The role of solvation in the binding selectivity of the
54 L-type calcium channel, *J. Chem. Phys.* **139**, 055103 (2013).
55 [65] Fraenkel, D., Computing excess functions of electrolyte solutions: The smaller-ion shell model

- versus the primitive model. Part 2 – Ion-size parameters, *J. Chem. Theor. Comp.* DOI: 10.1021/ct500694u (2014).
- [66] Koneshan, S., Rasaiah, J. C., Lynden-Bell, R. M. & Lee, S. H., Solvent structure, dynamics, and ion mobility in aqueous solutions at 25 C, *J. Phys. Chem. B* **102**, 4193–4204 (1998).
- [67] Parsegian, A., Energy of an ion crossing a low dielectric membrane: solutions to four relevant electrostatic problems, *Nature* **221**, 844–846 (1969).
- [68] Levitt, D. G., Electrostatic calculations for an ion channel. 1. Energy and potential profiles and interactions between ions, *Biophys. J.* **22**, 209–219 (1978).
- [69] Cheng, M. H. & Coalson, R. D., An accurate and efficient empirical approach for calculating the dielectric self-energy and ion-ion pair potential in continuum models of biological ion channels, *J. Phys. Chem. B* **109**, 488–498 (2005).
- [70] Vora, T., Corry, B. & Chung, S. H., A model of sodium channels, *Biochim. Biophys. Acta Biomem.* **1668**, 106–116 (2005).
- [71] Berti, C., Gillespie, D., Bardhan, J. P., Eisenberg, R. S. & Fiegna, C., Comparison of three-dimensional Poisson solution methods for particle-based simulation and inhomogeneous dielectrics, *Phys. Rev. E* **86**, 011912 (2012).
- [72] Tindjong, I. Kh. Kaufman, R., Luchinsky, D. G., McClintock, P. V. E., Khovanov, I. A. & Eisenberg, R. S., Non-equilibrium stochastic dynamics of open ion channels, *Nonlin. Phenom. Complex Syst.* **16**, 146–161 (2013).
- [73] Tindjong, R., Kaufman, I. K., Luchinsky, D. G., McClintock, P. V. E., Khovanov, I. & Eisenberg, R. S., Self-organized enhancement of conductivity in biological ion channels, *New J. Phys.* **15**, 103005 (2013).
- [74] Yesylevskyy, S. O. & Kharkyanen, V. N., Barrier-less knock-on conduction in ion channels: peculiarity or general mechanism?, *Chem. Phys.* **312**, 127–133 (2005).
- [75] Tieleman, D. P., Biggin, P. C., Smith, G. R. & Sansom, M. S. P., Simulation approaches to ion channel structure-function relationships, *Quart. Rev. Biophys.* **34**, 473–561 (2001).
- [76] Nelissen, K., Misko, V. R. & Peeters, F. M., Single-file diffusion of interacting particles in a one-dimensional channel, *EPL (Europhys. Lett.)* **80**, 56004 (2007).
- [77] Hess, P. & Tsien, R. W., Mechanism of ion permeation through calcium channels, *Nature* **309**, 453–456 (1984).
- [78] Armstrong, C. M. & Neyton, J., Ion permeation through calcium channels, *Ann. New York. Acad. Sci.* **635**, 18–25 (1991).
- [79] Nelson, P. H., A permeation theory for single-file ion channels: One- and two-step models, *J. Chem. Phys.* **134**, 165102–165114 (2011).
- [80] Reichl, L. E. & Prigogine, I., *A Modern Course in Statistical Physics* (University of Texas, Austin, 1980).
- [81] Alam, A. & Jiang, Y., Structural analysis of ion selectivity in the NaK channel, *Nat. Struct. Mol. Biol.* **16**, 35–41 (2008).
- [82] Furini, S., Barbini, P. & Domene, C., Effects of the protonation state of the EEEE motif of a bacterial Na⁺-channel on conduction and pore structure, *Biophys. J.* **106**, 2175–2183 (2014).
- [83] Dirac, P. A. M., *The Principles of Quantum Mechanics* (OUP, Oxford, 1930).
- [84] Kaniadakis, G. & Quarati, P., Kinetic equation for classical particles obeying an exclusion principle, *Phys. Rev. E* **48**, 4263–4270 (1993).
- [85] Liu, J.-L. & Eisenberg, R., Correlated ions in a calcium channel model: A Poisson-Fermi theory, *J. Phys. Chem. B* **117**, 12051–12058 (2013).
- [86] Fowler, R. H., A statistical derivation of Langmuir’s adsorption isotherm, in *Mathematical Proceedings of the Cambridge Philosophical Society*, vol. 31, 260–264 (CUP, Cambridge, 1935).
- [87] Zocchi, G., Controlling proteins through molecular springs, *Ann. Rev. Biophys.* **38**, 75–88 (2009).
- [88] Bezanilla, F. & Villalba-Galea, C. A., The gating charge should not be estimated by fitting a two-state model to a Q-V curve, *J. Gen. Physiol.* **142**, 575–578 (2013).
- [89] Liu, J.-L., Numerical methods for the Poisson-Fermi equation in electrolytes, *J. Comp. Phys.* **247**,

1
2
3 *Coulomb blockade model of permeation and selectivity in biological ion channels* 24
4

5 88–99 (2013).

- 6 [90] Liu, J.-L. & Eisenberg, B., Analytical models of calcium binding in a calcium channel, *J. Chem.*
7 *Phys.* **141**, 075102 (2014).
- 8 [91] Kubo, R., The fluctuation-dissipation theorem, *Rep. Prog. Phys.* **29**, 255 (1966).
- 9 [92] Kulik, I. O. & Shekhter, R. I., Kinetic phenomena and charge-discreteness effects in granulated
10 media, *Zh. Eksp. Teor. Fiz.* **68**, 623–640 (1975).
- 11 [93] Tindjong, R., Kaufman, I. K., McClintock, P. V. E., Luchinsky, D. G. & Eisenberg, R. S.,
12 Nonequilibrium rate theory for conduction in open ion channels, *Fluct. Noise Lett.* **11**, 1240016
13 (2012).
- 14 [94] Mott, N. F. & Gurney, R. W., *Electronic Processes in Ionic Crystals* (Clarendon Press, Oxford,
15 1957).
- 16 [95] Shockley, W., The path to the conception of the junction transistor, *IEEE Trans. Electron Dev.*
17 **23**, 597–620 (1976).
- 18 [96] Luchinsky, D. G. & McClintock, P. V. E., Irreversibility of classical fluctuations studied in analogue
19 electrical circuits, *Nature* **389**, 463–466 (1997).
- 20 [97] Barcion, V., Chen, D., Eisenberg, R. S. & Ratner, M. A., Barrier crossing with concentration
21 boundary conditions in biological channels and chemical reactions, *J. Chem. Phys.* **98**, 1193–
22 1212 (1993).
- 23 [98] Fox, J. A., Ion channel subconductance states, *J. Membrane Biol.* **97**, 1–8 (1987).
- 24
25
26
27
28
29
30
31
32
33
34
35
36
37
38
39
40
41
42
43
44
45
46
47
48
49
50
51
52
53
54
55
56
57
58
59
60